

Robust Quantum-MUSIC for DoA Estimation Using Rydberg Atomic Receiver Arrays

Sourav Banerjee , Neel Kanth Kundu , *Member, IEEE*, and Prajwalita Borah

Abstract—Quantum wireless sensing using Rydberg atomic receivers enables high-sensitivity signal acquisition direction-of-arrival (DoA) estimation. However, it suffers from a fundamental limitation, where only the magnitude of the received signal is observable. The recently proposed Quantum-MUSIC algorithm addresses this problem by recovering phase information through alternating minimization and subsequently applying the MUSIC algorithm for DoA estimation. However, the existing approach relies on an ℓ_2 -norm phase retrieval step, making it highly sensitive to outlier measurements produced by hardware faults, sensor saturation, or adversarial interference. In this letter, we propose a *Robust Quantum-MUSIC* (RobQMUSIC) framework that replaces the ℓ_2 -norm with an ℓ_1 -norm formulation. The resulting weighted phase-retrieval problem is solved efficiently via an Iteratively Reweighted Least Squares (IRLS) scheme embedded within the alternating minimization loop, requiring no increase in structural complexity relative to the baseline algorithm. Simulation results demonstrate that RobQMUSIC achieves near-identical DoA estimation accuracy to Quantum-MUSIC under ideal conditions, while maintaining robust performance over a wide range of outlier contamination levels at which Quantum-MUSIC fails entirely.

Index Terms—Rydberg atom RF sensor, robust DoA estimation, Quantum MUSIC, array processing

I. INTRODUCTION

Recent years have witnessed a paradigm shift from conventional wireless sensing toward quantum-enabled sensing, driven by the need for ultra-high sensitivity and precision in next-generation communication and radar systems [1], [2]. In particular, atomic RF receivers based on highly excited Rydberg states have emerged as a promising technology for quantum wireless sensing, owing to their ability to interact directly with electromagnetic fields over a broad frequency spectrum [3], [4]. Unlike classical antennas, these quantum RF sensors exploit the atom-field interactions to achieve exceptionally high sensitivity, thereby opening new avenues for high-resolution channel estimation and direction of arrival (DoA) sensing [5].

Despite growing interest, the integration of atomic receivers into practical wireless sensing systems remains at an early

The work of Neel Kanth Kundu was supported in part by the DST INSPIRE Faculty Fellowship (Reg. No.: IFA22-ENG 344), ANRF PM Early Career Research Grant (ANRF/ECRG/2024/000324/ENS), and IIT Delhi's New Faculty Seed Grant (MI02855G). (*Corresponding author: Neel Kanth Kundu.*)

Sourav Banerjee and Prajwalita Borah are with the Center for Applied Research in Electronics (CARE), Indian Institute of Technology (IIT) Delhi, New Delhi-110016, India (e-mail: crz248112@care.iitd.ac.in, crz248470@care.iitd.ac.in).

Neel Kanth Kundu is with CARE and Bharti School of Telecommunication Technology and Management, IIT Delhi, New Delhi, India. He is also an honorary fellow at the Department of Electrical and Electronic Engineering, University of Melbourne, Melbourne, VIC-3010, Australia (e-mail: neelkanth@iitd.ac.in).

stage. Existing works have primarily addressed simplified scenarios such as single-target sensing via geometric phase relationships [5]. While such approaches demonstrate feasibility, they fail to generalize to realistic multi-user environments. Although several experimental studies have validated quantum wireless sensing [6], accurate multi-user DoA estimation remains challenging owing to the magnitude-only measurement constraint of the Rydberg atomic RF receiver.

To address this challenge, Quantum-MUSIC was recently proposed as a signal-processing framework for multi-user quantum wireless sensing with atomic RF receivers [7]. The algorithm first recovers the channel matrix from magnitude-only measurements via a modified, biased Gerchberg-Saxton (GS) phase-retrieval procedure [8], followed by the application of the classical MUSIC algorithm [9] for multi-user DoA estimation. Numerical results in [7] demonstrated that Quantum-MUSIC outperforms conventional RF-domain MUSIC, establishing a foundational framework for Rydberg-atom-based DoA estimation problems.

A critical limitation of Quantum-MUSIC, however, is its sensitivity to measurement imperfections. In practice, atomic receiver outputs are corrupted by hardware malfunctions, sensor saturation, intermittent atomic-excitation failures, or adversarial interference, resulting in large-amplitude additive outliers in a sparse subset of measurements. Since the channel-recovery step of the Quantum-MUSIC algorithm minimizes an ℓ_2 -norm residual—which penalizes errors quadratically—even a small fraction of such outliers can dominate the cost and severely degrade the recovered channel matrix and the ensuing DoA estimates.

Robust estimation via ℓ_1 -norm minimization is a well-established remedy for outlier sensitivity [10], [11]. Linear penalization of residuals limits the influence of large outliers without sacrificing accuracy on inlier measurements. Although ℓ_1 problems are not directly solvable in closed form, the Iteratively Reweighted Least Squares (IRLS) algorithm provides a computationally tractable approximation by iteratively solving a sequence of diagonal-reweighted ℓ_2 problems [12], [13].

In this letter, we propose a robust extension of Quantum-MUSIC (RobQMUSIC) that replaces the ℓ_2 phase-retrieval step with an ℓ_1 -IRLS formulation. The proposed method retains the same spectral-method initialization and alternating-minimization structure as [7], adding only an inner IRLS loop that reweights each snapshot according to its current residual magnitude. This modification is simple to implement, adds negligible computational overhead per outer iteration, and confers strong robustness to sparse large-amplitude outliers.

Notation: Boldface lowercase and uppercase letters denote vectors and matrices, respectively. $(\cdot)^H$ and $(\cdot)^T$ denote conjugate transpose and transpose. $|\cdot|$ applied element-wise denotes

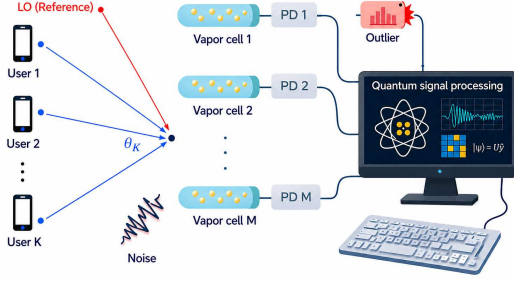


Fig. 1: Schematic of the multi-user DoA estimation system using Rydberg atomic receiver array in the presence of outliers.

the modulus; $\|\cdot\|_1$ and $\|\cdot\|_2$ denote the ℓ_1 - and ℓ_2 -norms. \odot and \circ denote the Hadamard (element-wise) product. $\mathcal{CN}(\boldsymbol{\mu}, \sigma^2 \mathbf{I})$ denotes a circularly-symmetric complex Gaussian distribution.

II. QUANTUM PHYSICS OF THE RYDBERG ATOMIC RECEIVER

For completeness, we briefly review the relevant Rydberg atom physics principles from [7]. In the considered system, K single-antenna users transmit RF signals to an atomic receiver array comprising M vapor cells, each filled with Rydberg atoms. Unlike conventional receivers, information is not processed in the electrical domain; instead it is encoded in the quantum-state transitions of the atoms. The total EM field incident on the m -th vapor cell is formed by the superposition of all users' signals:

$$E_m(t) = \sum_{k=1}^K \epsilon \sqrt{P_k} \rho_k s_k \cos(\omega t + \varphi_{m,k}), \quad (1)$$

where ϵ , ρ_k , $\varphi_{m,k}$, P_k , and s_k denote the polarization direction, path loss, phase shift, transmit power, and transmitted signal of the k -th user at the m -th cell, respectively. This field drives quantum-state transitions whose strength is characterised by the *Rabi frequency*, observable via electromagnetically induced transparency (EIT) and Autler–Townes (AT) splitting [14]. The Rabi frequency at the m -th cell is

$$\Omega_m = \left| \sum_{k=1}^K \frac{1}{\hbar} \boldsymbol{\mu}_{eg}^H \epsilon \sqrt{P_k} \rho_k s_k e^{-j\varphi_{m,k}} \right|, \quad (2)$$

where \hbar is the reduced Planck constant and $\boldsymbol{\mu}_{eg}$ is the transition dipole moment. Equation (2) shows that the Rabi frequency inherently encodes the full channel—power, path loss, phase shift, and polarization—transforming the classical RF reception problem into a quantum measurement problem whose output is a *magnitude-only* observable.

III. SYSTEM MODEL

A. Signal and Channel Model

As shown in Fig. 1, K users transmit signals toward a uniform linear array (ULA) made of Rydberg receivers. A local oscillator (LO) is also present as a reference signal. These RF signals are converted into optical responses via the

interaction of electromagnetic fields with Rydberg atoms in vapor cells. The optical signals are detected by photodetectors (PDs), producing electrical measurement signals.

Let $\mathbf{s} \in \mathbb{C}^K$ be the transmitted signal vector. The complex baseband signal at the m -th sensor is

$$y_m = \mathbf{s}^H \mathbf{h}_m + b_m + n_m, \quad (3)$$

where $\mathbf{h}_m \in \mathbb{C}^K$ is the channel vector, $b_m = \frac{1}{\hbar} \boldsymbol{\mu}_{eg}^H \epsilon_{LO} \sqrt{P_b} \in \mathbb{C}$ is a known deterministic bias from the LO reference, and $n_m \sim \mathcal{CN}(0, \sigma_n^2)$ is the quantum shot noise (QSN). Here, the relation between the Rabi frequency and complex baseband signal is $\Omega_m = |y_m|$.

B. Steering-Vector Parametrization

Assuming a narrowband signal in the far-field propagation and a ULA with half-wavelength spacing $d = \lambda/2$, the channel vector of the k -th user is the steering vector

$$\mathbf{a}(\theta_k) = \alpha [1, e^{-j\pi \sin \theta_k}, \dots, e^{-j\pi(M-1) \sin \theta_k}]^T \in \mathbb{C}^M, \quad (4)$$

where θ_k is the DoA of the k -th user and $\alpha = \frac{1}{\hbar} \boldsymbol{\mu}_{eg}^H \epsilon \sqrt{P_k} \rho_k$ subsumes path loss and polarization. Stacking all K steering vectors gives the array manifold matrix $\mathbf{A}(\boldsymbol{\theta}) = [\mathbf{a}(\theta_1), \dots, \mathbf{a}(\theta_K)] \in \mathbb{C}^{M \times K}$, which can also be expressed as follows:

$$\mathbf{A}(\boldsymbol{\theta}) = \begin{bmatrix} -\mathbf{h}_1^T & - \\ -\mathbf{h}_2^T & - \\ \vdots & \\ -\mathbf{h}_M^T & - \end{bmatrix} \quad (5)$$

By performing channel estimation, the DoA vector $\boldsymbol{\theta} = [\theta_1, \dots, \theta_K]^T$ can be further estimated.

C. Multi-Snapshot Magnitude-Only Measurement Model

Collecting P independent pilot snapshots, the pilot matrix is given by $\mathbf{S} = [\mathbf{s}_1, \dots, \mathbf{s}_P] \in \mathbb{C}^{K \times P}$. Stacking all sensor outputs yields the *measurement matrix*

$$\mathbf{Z} = [\mathbf{Z}_{:,1}, \dots, \mathbf{Z}_{:,P}] \in \mathbb{R}_+^{M \times P}, \quad \mathbf{Z}_{:,p} = |\mathbf{A}(\boldsymbol{\theta}) \mathbf{s}_p + \mathbf{b} + \mathbf{n}_p|, \quad (6)$$

where the modulus is applied element-wise. Equivalently, \mathbf{z}_m^T is the m -th row that satisfies $\mathbf{z}_m = |\mathbf{S}^H \mathbf{h}_m + \mathbf{b}_m + \mathbf{n}_m|$, where $\mathbf{b}_m = b_m \mathbf{1}_P$.

D. Corrupted Measurement Model

In practice, a sparse subset of entries of \mathbf{Z} is corrupted due to hardware faults, saturation, or interference. Let $\mathcal{S} \subset \{1, \dots, M\} \times \{1, \dots, P\}$ be the unknown support set with $|\mathcal{S}| = S \ll MP$. The observed matrix is

$$\tilde{\mathbf{Z}} = \mathbf{Z} + \mathbf{E}, \quad (7)$$

where $\mathbf{E} \in \mathbb{R}^{M \times P}$ is a sparse matrix with $E_{m,p} \neq 0$ iff $(m, p) \in \mathcal{S}$. The non-zero entries represent *outliers* of arbitrary magnitude and sign with no assumed distribution. Because ℓ_2 -based channel recovery is sensitive to such large-magnitude

corruption, we formulate the channel estimation problem as an ℓ_1 -norm minimization:

$$\min_{\mathbf{h}_m} \|\tilde{\mathbf{z}}_m - \mathbf{S}^H \mathbf{h}_m + \mathbf{b}_m\|_1, \quad m = 1, \dots, M, \quad (8)$$

where $\tilde{\mathbf{z}}_m^T$ denotes the m -th row of $\tilde{\mathbf{Z}}$.

IV. PROPOSED ROBUST QUANTUM-MUSIC ALGORITHM

A. Alternating Minimization Formulation

Problem (8) is non-convex due to the modulus operator. Following [7], we introduce an auxiliary phase vector $\angle \mathbf{u}_m$ and reformulate the problem as the alternating minimization

$$\min_{\mathbf{h}_m, \angle \mathbf{u}_m} \|\tilde{\mathbf{z}}_m \circ e^{j\angle \mathbf{u}_m} - \mathbf{S}^H \mathbf{h}_m - \mathbf{b}_m\|_1, \quad (9)$$

which decouples into a *phase update* and an *amplitude update* step, each convex when the other is fixed.

B. Spectral Initialisation

To avoid convergence to poor local minima, the channel estimate is initialised using the spectral method of [15]. Define the expanded signal matrix $\bar{\mathbf{S}} = [\mathbf{S}^H, \mathbf{b}_m]^H \in \mathbb{C}^{(K+1) \times P}$ and the expanded channel vector $\bar{\mathbf{h}}_m = [\mathbf{h}_m^H, 1]^H \in \mathbb{C}^{K+1}$. The expanded covariance matrix is

$$\bar{\mathbf{R}} = \sum_{p=1}^P \bar{z}_{m,p} \bar{s}_p \bar{s}_p^H \in \mathbb{C}^{(K+1) \times (K+1)}. \quad (10)$$

Letting \mathbf{v} be the principal eigenvector of $\bar{\mathbf{R}}$, the initial estimate is $\bar{\mathbf{a}}_m^0 = \bar{r} \mathbf{v}$ with scalar $\bar{r} = |\mathbf{v}^H \bar{\mathbf{S}}| \tilde{\mathbf{z}}_m| / \|\bar{\mathbf{S}}^H \mathbf{v}\|_2^2$, and $\mathbf{h}_m^0 = \bar{\mathbf{h}}_m^0(1 : K)$.

C. Phase Update

For fixed \mathbf{h}_m^{n-1} , the phase update is obtained as

$$\angle \mathbf{u}_m^n = \angle(\mathbf{S}^H \mathbf{h}_m^{n-1} + \mathbf{b}_m), \quad (11)$$

and setting $\tilde{\mathbf{z}}_m^n = \tilde{\mathbf{z}}_m \circ e^{j\angle \mathbf{u}_m^n}$.

D. Amplitude Update via IRLS

For fixed $\tilde{\mathbf{z}}_m^n$, (9) reduces to the ℓ_1 weighted least-squares problem

$$\min_{\mathbf{h}_m} \|\tilde{\mathbf{z}}_m^n - \mathbf{S}^H \mathbf{h}_m - \mathbf{b}_m\|_1. \quad (12)$$

We solve (12) via IRLS, which iterates the following two substeps for $t = 1, \dots, T$:

- 1) **Weight update:** Compute the residual $\varrho^{(t)} = \tilde{\mathbf{z}}_m^n - \mathbf{S}^H \mathbf{h}_m^{n(t)} - \mathbf{b}_m$ and set diagonal weights

$$w_p^{(t+1)} = \frac{1}{|\varrho_p^{(t)}| + \epsilon}, \quad p = 1, \dots, P, \quad (13)$$

where $\epsilon > 0$ is a small regularization constant that prevents division by zero and also stabilizes convergence near the solution. Entries with large residuals—corresponding to outliers—receive small weights and are thus down-weighted in the subsequent step.

- 2) **Weighted least-squares solution:**

$$\mathbf{h}_m^{n(t+1)} = (\mathbf{S}^H \mathbf{W}^{(t)} \mathbf{S}^H)^{-1} \mathbf{S}^H \mathbf{W}^{(t)} (\tilde{\mathbf{z}}_m^n - \mathbf{b}_m), \quad (14)$$

where $\mathbf{W}^{(t)} = \text{diag}(w_1^{(t)}, \dots, w_P^{(t)})$.

After T IRLS iterations, the amplitude estimate is set to $\mathbf{h}_m^n = \mathbf{h}_m^{n(T)}$.

E. DoA Estimation via MUSIC

After N outer iterations yield $\hat{\mathbf{h}}_m = \mathbf{h}_m^N$ for all m , the estimated channel matrix $\hat{\mathbf{H}} = [\hat{\mathbf{h}}_1, \dots, \hat{\mathbf{h}}_M]^H$ is used to form the sample covariance matrix

$$\mathbf{R} = \frac{1}{P} \hat{\mathbf{H}} \hat{\mathbf{H}}^H \in \mathbb{C}^{M \times M}. \quad (15)$$

Eigenvalue decomposition of \mathbf{R} yields the signal and noise subspaces $\mathbf{U}_S \in \mathbb{C}^{M \times K}$ and $\mathbf{U}_N \in \mathbb{C}^{M \times (M-K)}$, respectively. For an ULA with M sensors, inter-element spacing $d \approx \frac{\lambda}{2}$, and wavelength λ , the far-field steering vector is given by $\mathbf{a}(\theta) = \frac{1}{\sqrt{M}} [1 \ e^{j\pi \sin \theta} \ e^{j2\pi \sin \theta} \ \dots \ e^{j(M-1)\pi \sin \theta}]$. The Quantum-MUSIC pseudo-spectrum is given by

$$P_Q(\theta) = \frac{1}{\mathbf{a}^H(\theta) \mathbf{U}_N \mathbf{U}_N^H \mathbf{a}(\theta)}, \quad (16)$$

and the DoA estimates $\{\hat{\theta}_k\}_{k=1}^K$ are identified as the K largest peaks of $P_Q(\theta)$.

The complete robust quantum MUSIC procedure is summarized in Algorithm 1.

F. Computational Complexity

The computational complexity of RobQMUSIC consists of four main stages. Spectral initialization, including construction of the expanded covariance matrices and principal eigenvector extraction for all M sensors, requires $\mathcal{O}(MK^2P)$. The phase update step costs $\mathcal{O}(KP)$ per sensor per outer iteration, leading to a total complexity of $\mathcal{O}(MNKP)$. For the IRLS amplitude update, each inner iteration is dominated by forming the weighted normal matrix and solving a $K \times K$ system, resulting in complexity $\mathcal{O}(K^2P + K^3)$; with T IRLS iterations over N outer iterations and M sensors, the total cost becomes $\mathcal{O}(MNT(K^2P + K^3))$. The final MUSIC spectral search, including covariance formation, eigendecomposition, and pseudo-spectrum evaluation over G_θ grid points, requires $\mathcal{O}(M^3 + G_\theta M^2)$. Therefore, the overall computational complexity of RobQMUSIC is dominated by

$$\mathcal{O}(M(K^3 + NTPK^2 + M^2 + G_\theta M)). \quad (17)$$

Compared with Quantum-MUSIC [7], RobQMUSIC introduces only an additional multiplicative factor T in the phase-retrieval stage. Since T is a small fixed constant and typically $K \ll P$, this additional overhead is negligible while providing improved robustness.

V. NUMERICAL RESULTS

A. Simulation Setup

We evaluate RobQMUSIC against Quantum-MUSIC of [7] using the same physical parameters. Rydberg energy levels $52D_{5/2}$ and $53P_{3/2}$ of the Caesium (Cs) atom detect RF signals at $\omega_{eg} \approx 2\pi \times 5$ GHz. The transition dipole moment is obtained via the ARC package [16] as $\boldsymbol{\mu}_{eg} = [0, 1785.9 \text{ qa}_0, 0]^T$,

Algorithm 1 Robust Quantum-MUSIC (RobQMUSIC)

Input: \mathbf{S} , \mathbf{b} , $\tilde{\mathbf{Z}}$, N , T , ϵ
Output: $\{\hat{\theta}_k\}_{k=1}^K$ from K largest peaks of $P_Q(\theta)$

```

1: for  $m = 1$  to  $M$  do
2:   Form  $\tilde{\mathbf{S}} = [\mathbf{S}^H, \mathbf{b}_m]^H$ ; compute  $\tilde{\mathbf{R}}$  via (10)
3:   Obtain  $\mathbf{h}_m^0$  via spectral initialisation (Section IV-B)
4:   for  $n = 1$  to  $N$  do
5:     Phase update:  $\tilde{\mathbf{z}}_m^n \leftarrow \tilde{\mathbf{z}}_m \circ e^{j\angle(\mathbf{S}^H \mathbf{h}_m^{n-1} + \mathbf{b}_m)}$ 
6:     Initialise  $w_p^{(1)} = 1$ ,  $p = 1, \dots, P$ 
7:     for  $t = 1$  to  $T$  do
8:       Compute residual  $\boldsymbol{\rho}^{(t)} = \tilde{\mathbf{z}}_m^n - \mathbf{S}^H \mathbf{h}_m^{n(t)} - \mathbf{b}_m$ 
9:       Update weights via (13)
10:      Solve WLS via (14) to obtain  $\mathbf{h}_m^{n(t+1)}$ 
11:      if  $\frac{\|\mathbf{h}_m^{n(t+1)} - \mathbf{h}_m^{n(t)}\|_2}{\|\mathbf{h}_m^{n(t)}\|_2 + \epsilon} < 10^{-8}$  then
12:        break
13:      end if
14:    end for
15:     $\mathbf{h}_m^n \leftarrow \mathbf{h}_m^{n(T)}$ 
16:  end for
17:   $\hat{\mathbf{h}}_m \leftarrow \mathbf{h}_m^N$ 
18: end for
19: Form  $\hat{\mathbf{H}} = [\hat{\mathbf{h}}_1, \dots, \hat{\mathbf{h}}_M]^H$ ; compute  $\mathbf{R}$  via (15)
20: Compute noise subspace  $\mathbf{U}_N$ ; evaluate  $P_Q(\theta)$  via (16)
  
```

TABLE I: Simulation Parameters

Parameter	Fig. 2	Fig. 3	Fig. 4
Array size M	32	32	8
Snapshots P	100	500	200
Monte Carlo MC	1	100	500
Corruption η (%)	0, 20	0–90	0, 25
Outlier magnitude δ	3	10	39
IRLS ϵ	10^{-8}		

where $q = 1.602 \times 10^{-19}$ C and $a_0 = 5.292 \times 10^{-11}$ m. Polarization directions ϵ and ϵ_{LO} are i.i.d. $\mathcal{N}(0, \frac{1}{3})$, and the LO reference power is $P_b = 10P_k$. The pilot matrix $\mathbf{S} \in \mathbb{C}^{K \times P}$ has i.i.d. $\mathcal{CN}(0, 1)$ entries. Throughout, we assume $K = 2$ users, and they have true DoAs $\theta_1 = 40^\circ$ and $\theta_2 = -60^\circ$, and the angular search grid contains $G_\theta = 2000$ points on $[-90^\circ, 90^\circ]$.

Three experiments are conducted and their specific parameters are listed in Table I. For the corruption sweep and spectrum comparison, P_k and σ_n^2 are fixed at ($P_k = 10^{-18}$ and $\sigma_n^2 = 10^{-19.1}$). For the SNR sweep, $P_k = 10^{-18}$ and $SNR = \frac{P_k \mu_{eg}(2)^{\frac{1}{3h}}}{\sigma_n^2}$ and we vary σ_n^2 to set the SNR value from 0 to 20 dB with an interval of 4dB. Outliers are injected by selecting a fraction η of entries of \mathbf{Z} uniformly at random and perturbing each by $\pm\delta$, following (7) as done in [17], therefore making all the non-zero elements of \mathbf{E} as $\pm\delta$. The RMSE is

$$\text{RMSE} = \sqrt{\frac{1}{MC \cdot K} \sum_{t=1}^{MC} \sum_{k=1}^K (\hat{\theta}_k^{(t)} - \theta_k)^2} \quad (18)$$

where MC denotes the number of Monte-Carlo runs.

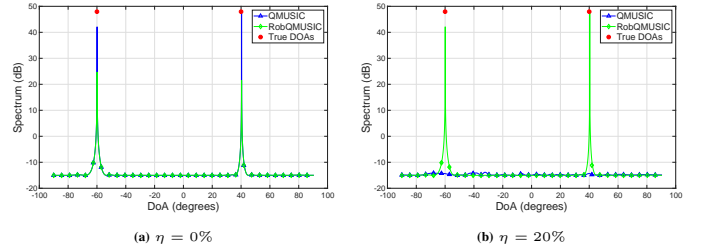


Fig. 2: MUSIC and RobQMUSIC pseudo-spectrum for two different corruption levels.

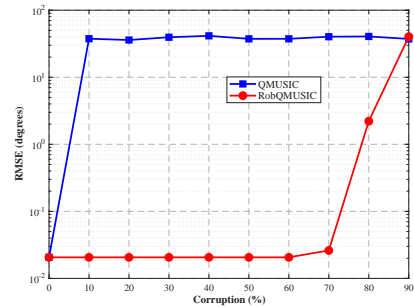
B. MUSIC Spectrum Under Outlier Corruption

Fig. 2 compares the MUSIC pseudo-spectra for a single realisation at $\eta = 0\%$ and $\eta = 20\%$. At $\eta = 0\%$ (Fig. 2a), both algorithms produce sharp, well-separated peaks precisely aligned with the true DoAs at 40° and -60° . The spectral profiles are nearly indistinguishable, confirming that the ℓ_1 -IRLS formulation does not incur a significant performance penalty in the absence of outliers.

At $\eta = 20\%$ (Fig. 2b), the contrast is stark. QMUSIC, which minimizes a quadratic residual, is overwhelmed by the large-amplitude outliers: its spectrum is severely distorted and fails entirely to resolve the two sources. RobQMUSIC retains sharp, correctly located peaks at both DoAs, demonstrating that the IRLS weight updates effectively isolate the outlier-contaminated snapshots and preserve the signal-subspace structure required for accurate MUSIC-based DoA estimation.

C. RMSE Versus Outlier Fraction

Fig. 3 shows the RMSE as a function of the outlier fraction $\eta \in \{0, 10, \dots, 90\}\%$ at $\frac{P_k}{\sigma_n^2} \approx 11$ dB. At $\eta = 0\%$, both algorithms achieve $\text{RMSE} \approx 0.02^\circ$, confirming parity under ideal conditions. As η increases, QMUSIC degrades rapidly: the RMSE saturates near 40° for all $\eta \geq 20\%$, indicating consistent failure to estimate the DoA of the two sources. RobQMUSIC maintains $\text{RMSE} \approx 0.02^\circ$ across the entire range $\eta \in [0\%, 70\%]$. After $\eta = 70\%$, the algorithm fails to estimate the DoAs and loses its robustness.

Fig. 3: RMSE vs. outlier fraction η

D. RMSE Versus SNR

Figs. (4a) and (4b) show the RMSE versus SNR at $\eta = 0\%$ and $\eta = 25\%$, respectively ($M = 8$, $P = 200$, $MC = 500$).

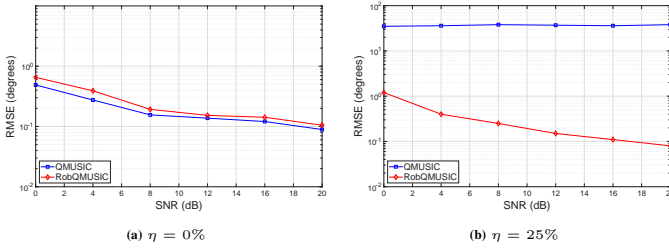


Fig. 4: RMSE vs. SNR comparison under clean and corrupted measurements.

1) *No Outliers ($\eta = 0\%$)*: Both algorithms improve monotonically with SNR. QMUSIC achieves lower RMSE throughout which decreases with increasing SNR. RobQMUSIC follows the same trend with a slightly higher RMSE at each SNR value. This gap reflects the inherent statistical efficiency cost of ℓ_1 penalisation: IRLS down-weights small-residual inliers alongside outliers, raising the effective noise floor. Nevertheless, both curves converge asymptotically at high SNR, where the channel estimate is accurate enough that few snapshots are misidentified as outliers.

2) *25% Outlier Corruption ($\eta = 25\%$)*: The situation reverses entirely under 25% corruption. QMUSIC saturates at $\approx 35^\circ$ RMSE across the full SNR range, confirming that the outlier energy completely dominates the ℓ_2 cost regardless of the operating SNR. RobQMUSIC improves monotonically from $\approx 1.2^\circ$ at SNR = 0 dB to $\approx 0.07^\circ$ at SNR = 20 dB.

Taken together, these experiments establish that RobQMUSIC achieves a favorable robustness-efficiency trade-off. It incurs a modest RMSE overhead relative to QMUSIC in the corruption-free regime, in exchange for near-complete immunity to sparse large-amplitude outliers—a trade-off that strongly benefits practical quantum wireless sensing systems.

VI. CONCLUSION

In this letter, we have proposed RobQMUSIC, a robust extension of the Quantum-MUSIC algorithm for DoA estimation with Rydberg atomic receiver arrays. By replacing the ℓ_2 -norm phase-retrieval step with an ℓ_1 -IRLS formulation, the proposed algorithm effectively suppresses the influence of sparse large-amplitude outliers without altering the overall alternating-minimization structure or introducing significant computational overhead. Our numerical simulation results reveal that RobQMUSIC maintains near-identical accuracy to Quantum-MUSIC under ideal conditions and achieves reliable DoA estimation up to 80% outlier contamination—a regime in which Quantum-MUSIC degrades to near-worst-case error. Future works will focus on wideband quantum wireless sensing scenarios, as well as investigating advanced array geometries capable of estimating a larger number of sources than the number of physical elements under magnitude-only measurements.

ACKNOWLEDGMENT

The authors would like to thank Prof. Prabhu Babu and Dr. Aakash Arora (CARE, IIT Delhi) for their valuable suggestions and insightful discussions that contributed to this work.

REFERENCES

- [1] Y. Chen, X. Guo, C. Yuen, Y. Zhao, Y. L. Guan, C. M. S. See, M. D ebbah, and L. Hanzo, "Harnessing Rydberg Atomic Receivers: From Quantum Physics to Wireless Communications," 2026. [Online]. Available: <https://arxiv.org/abs/2501.11842>
- [2] S. Banerjee and N. K. Kundu, "Rydberg Atomic RF Sensor-based Quantum Radar," in *2026 IEEE Applied Sensing Conference (APSCON)*, 2026, pp. 1–4.
- [3] D. A. Anderson, R. E. Sapiro, and G. Raithele, "An Atomic Receiver for AM and FM Radio Communication," *IEEE Transactions on Antennas and Propagation*, vol. 69, no. 5, pp. 2455–2462, 2021.
- [4] C. T. Fancher, D. R. Scherer, M. C. S. John, and B. L. S. Marlow, "Rydberg Atom Electric Field Sensors for Communications and Sensing," *IEEE Transactions on Quantum Engineering*, vol. 2, pp. 1–13, 2021.
- [5] A. K. Robinson, N. Prajapati, D. Senic, M. T. Simons, and C. L. Holloway, "Determining the Angle-of-Arrival of a Radio-Frequency Source with a Rydberg Atom-Based Sensor," *Applied Physics Letters*, vol. 118, no. 11, p. 114001, 2021.
- [6] R. Mao, Y. Lin, Y. Fu, Y. Ma, and K. Yang, "Digital Beamforming and Receiving Array Research Based on Rydberg Field Probes," *IEEE Transactions on Antennas and Propagation*, vol. 72, no. 2, pp. 2025–2029, 2024.
- [7] H. Kim, H. Park, and S. Kim, "Quantum-MUSIC: Multiple Signal Classification for Quantum Wireless Sensing," *IEEE Wireless Communications Letters*, vol. 14, no. 6, pp. 1623–1627, 2025.
- [8] M. Cui, Q. Zeng, and K. Huang, "Towards Atomic MIMO Receivers," *IEEE Journal on Selected Areas in Communications*, vol. 43, no. 3, pp. 659–673, 2025.
- [9] R. Schmidt, "Multiple emitter location and signal parameter estimation," *IEEE Transactions on Antennas and Propagation*, vol. 34, no. 3, pp. 276–280, 1986.
- [10] E. J. Cand es and M. B. Wakin, "An Introduction To Compressive Sampling," *IEEE Signal Processing Magazine*, vol. 25, no. 2, pp. 21–30, 2008.
- [11] S. Boyd and L. Vandenberghe, *Convex Optimization*. Cambridge University Press, 2004.
- [12] I. Daubechies, R. DeVore, M. Fornasier, and C. S. G unt urk, "Iteratively Reweighted Least Squares Minimization for Sparse Recovery," *Communications on Pure and Applied Mathematics*, vol. 63, no. 1, pp. 1–38, 2010.
- [13] M.-J. Lai, Y. Xu, and W. Yin, "Improved Iteratively Reweighted Least Squares for Unconstrained Smoothed ℓ_q Minimization," *SIAM Journal on Numerical Analysis*, vol. 51, no. 2, pp. 927–957, 2013.
- [14] B. Liu, L.-H. Zhang, Z.-K. Liu, Z.-Y. Zhang, Z.-H. Zhu, W. Gao, G.-C. Guo, D.-S. Ding, and B.-S. Shi, "Electric Field Measurement and Application Based on Rydberg Atoms," *Electromagnetic Science*, vol. 1, no. 1, pp. 1–16, 2023.
- [15] E. J. Cand es, X. Li, and M. Soltanolkotabi, "Phase Retrieval via Wirtinger Flow: Theory and Algorithms," *IEEE Transactions on Information Theory*, vol. 61, no. 4, pp. 1985–2007, 2015.
- [16] N. Sibalic, J. D. Pritchard, C. S. Adams, and K. J. Weatherill, "ARC: an Open-Source Library for Calculating Properties of Alkali Rydberg Atoms," *Computer Physics Communications*, vol. 220, pp. 319–331, 2017.
- [17] P. Rajpurohit, P. Babu, and P. Stoica, "Robust Direction-of-Arrival Estimation in the Presence of Outliers," *IEEE Transactions on Aerospace and Electronic Systems*, vol. 61, no. 4, pp. 10921–10927, 2025.